doi:10.1093/brain/awx300 BRAIN 2018: 141; 205–216 | 205

BRAIN
A JOURNAL OF NEUROLOGY

A human prefrontal-subthalamic circuit for cognitive control

Ryan Kelley,[1,2,*] Oliver Flouty,[3,*] Eric B. Emmons,[2] Youngcho Kim,[4] Johnathan Kingyon,[5] Jan R. Wessel,[4] Hiroyuki Oya,[3] Jeremy D. Greenlee[3] and Nandakumar S. Narayanan[4]

*These authors contributed equally to this work.

The subthalamic nucleus is a key site controlling motor function in humans. Deep brain stimulation of the subthalamic nucleus can improve movements in patients with Parkinson's disease; however, for unclear reasons, it can also have cognitive effects. Here, we show that the human subthalamic nucleus is monosynaptically connected with cognitive brain areas such as the prefrontal cortex. Single neurons and field potentials in the subthalamic nucleus are modulated during cognitive processing and are coherent with 4-Hz oscillations in medial prefrontal cortex. These data predict that low-frequency deep brain stimulation may alleviate cognitive deficits in Parkinson's disease patients. In line with this idea, we found that novel 4-Hz deep brain stimulation of the subthalamic nucleus improved cognitive performance. These data support a role for the human hyperdirect pathway in cognitive control, which could have relevance for brain-stimulation therapies aimed at cognitive symptoms of human brain disease.

1 Medical Scientist Training Program, University of Iowa, Iowa City, IA 52242, USA
2 Program in Neuroscience, University of Iowa, Iowa City, IA 52242, USA
3 Department of Neurosurgery, University of Iowa, Iowa City, IA 52242, USA
4 Department of Neurology, University of Iowa, Iowa City, IA 52242, USA
5 Carver College of Medicine, University of Iowa, Iowa City, IA 52242, USA

Correspondence to: Jeremy D. Greenlee
Department of Neurosurgery, University of Iowa, Iowa City, IA 52242, USA
E-mail: jeremy-greenlee@uiowa.edu

Correspondence may also be addressed to: Nandakumar S. Narayanan
E-mail: nandakumar-narayanan@uiowa.edu

Keywords: hyperdirect pathway; subthalamic nucleus; cognitive control; deep brain stimulation; Parkinson's disease

Abbreviations: DBS = deep brain stimulation; ECoG = electrocorticography; ESTT = electrical stimulation tract-tracing; LFP = local field potential; PFC = prefrontal cortex; STN = subthalamic nucleus

Introduction

The human subthalamic nucleus (STN) is a key site of functional convergence from motor circuits (Alexander and Crutcher, 1990). As a result, the STN is a powerful therapeutic target for movement disorders such as Parkinson's disease (Limousin *et al.*, 1998; Follett, 2004). STN modulation with high-frequency deep brain stimulation (DBS) improves motor function (Limousin *et al.*, 1998; Follett *et al.*, 2010). In addition to input from indirect basal ganglia pathways, the STN is thought to receive fast monosynaptic projections directly from motor areas of the frontal cortex via a 'hyperdirect' pathway (Nambu *et al.*, 2002). Existence of this pathway has been demonstrated in non-human primates and rodents (Haynes and Haber, 2013; Averbeck *et al.*, 2014).

Received June 27, 2017. Revised September 5, 2017. Accepted September 25, 2017. Advance Access publication November 28, 2017

STN-DBS in humans has been proposed to involve these hyperdirect projections (Gradinaru *et al.*, 2009; Chiken and Nambu, 2014). However, hyperdirect projections from the frontal cortex to the STN have never been demonstrated in human intracranial recordings.

STN-DBS affects cognitive function (Heo *et al.*, 2008; Benabid *et al.*, 2009; Okun *et al.*, 2009). Multiple lines of evidence suggest that the STN is critically involved in inhibiting premature responses and regulation decision thresholds, including data from rats (Baunez and Robbins, 1997), non-human primates (Isoda and Hikosaka, 2008) and humans (Aron and Poldrack, 2006; Frank, 2006; Aron *et al.*, 2007; Jahfari *et al.*, 2012; Zaghloul *et al.*, 2012; Frank *et al.*, 2015). These studies have linked midfrontal EEG to STN activity (Cavanagh *et al.*, 2011; Zavala *et al.*, 2014; Frank *et al.*, 2015) and cognitive control (Aron *et al.*, 2007; Voon and Fox, 2007; Jahfari *et al.*, 2012; Herz *et al.*, 2016, 2017). Non-human primate studies have shown that the STN receives convergent hyperdirect input from cognitive frontal cortical areas such as the prefrontal cortex (PFC) (Haynes and Haber, 2013; Averbeck *et al.*, 2014; Alkemade *et al.*, 2015). STN local field potentials (LFPs) can have low-frequency coherence with prefrontal areas in delta and theta bands between 1 and 8 Hz (Zavala *et al.*, 2014). These data lead to the hypothesis that human hyperdirect low-frequency interactions between PFC and STN support cognitive control.

We tested this hypothesis via a novel combination of human neuroscience methods to directly measure PFC-STN connectivity in human patients undergoing neurosurgical treatment. In these patients, we demonstrate that lateral and medial areas of PFC are functionally connected with the STN. We probed PFC and STN activity in human neurosurgical patients using an interval-timing task. Interval timing is reliably disrupted in patients with Parkinson's disease and involves executive functions such as working memory for temporal rules as well as attention to the passage of time (Parker *et al.*, 2013, 2015; Kim *et al.*, 2017). We found that 4-Hz PFC oscillations interact with STN LFPs and single neurons during interval timing. Furthermore, we found that 4-Hz STN-DBS improved interval timing performance. Together, these data suggest the involvement of a hyperdirect fronto-basal ganglia pathway in cognitive functions in humans.

Materials and methods

Participants

Patients from the UIHC Neurology and Neurosurgery clinic participated under procedures approved by the University of Iowa's Institutional Review Board. In total, data from 13 patients with Parkinson's disease undergoing STN-DBS implantation were included: five patients for intraoperative electrical stimulation tract-tracing (ESTT) to map frontal-STN connectivity and 10 patients with intraoperative single-unit recordings, STN LFPs, and EEG activity from midfrontal electrodes (Supplementary Tables 2–4). Ten separate STN-DBS patients were included in EEG recordings during interval timing as STN-DBS parameters were changed; these patients were stable on DBS settings and levodopa for at least 1 month and were >3 months out from DBS implantation. In addition, three patients undergoing surgical treatment of medically intractable epilepsy with medial PFC electrocorticography (ECoG) coverage were included in this study; two for electrical stimulation-functional MRI and one for medial PFC ECoG recording during interval timing. All patients completed an extensive pre-surgical assessment, which included a detailed neurological examination, structural MRI, and neuropsychological evaluations that confirmed normal speech and language functions. ECoG patients had undergone WADA testing as well as had additional MRI, SPECT, and PET scans according to procedures described in detail previously (Kingyon *et al.*, 2015).

Bidirectional electrical stimulation tract-tracing

Once the DBS and subdural frontal ECoG strip electrodes were positioned over lateral PFC (specifically middle frontal gyrus) on both sides of the brain, bipolar constant voltage stimulation of two DBS contacts spanning dorsal STN was performed at 2.5, 5, and 10 V using single charged balanced 400-μs pulses with a fixed interstimulus interval of 1 s. A subgaleal strip electrode placed at the vertex served as a reference. All voltages are plotted with negative polarity as down. Multichannel continuous time series were digitized using Tucker-Davis Technology (TDT) RZ-2 acquisition system and stored for offline analysis. Trials were broken down to 1.5-s epochs constituting −0.5 s to +1 s relative to the electrical stimulus. Evoked potentials were calculated across trials for each contact and stimulation voltage. Significant early peak latencies were determined by false discovery rate-corrected repeated measures two-way *t*-test of voltages in 1 ms post-stimulation time bins versus mean baseline voltage (−100 to −1 ms from stimulation). Knowledge of the exact location of the surgical burr hole, direction of the strip (parallel to the superior sagittal sinus) and length the strip was slid posteriorly from the burr hole was accomplished by a combination of lateral fluoroscopy, intraoperative video, and direct observation of the attending neurosurgeon. This allowed for localization of the four electrode contacts on lateral PFC and motor cortex (Supplementary Fig. 1).

Human interval timing task

Interval timing was investigated in patients with Parkinson's disease undergoing STN-DBS implantation or with existing STN-DBS according to methods described in detail previously with a few modifications (Parker *et al.*, 2015). To be maximally compatible with the operating room, auditory stimuli were used. Briefly, trials started with an instructional cue (a recorded voice stating the word 'three' or 'twelve') followed 1 s later by an 8-kHz tone ('starting cue') indicating the start of the interval. Patients made responses by pressing a button on a button-box or a space bar on a keyboard using the hand

ipsilateral to the STN recording electrode. The first response after the start of the interval was recorded and a 3-s intertrial interval preceded the next trial. In the operating room, each block consisted of 40 trials. Participants performed a full block of practice trials in the operating room prior to the real task.

An identical task was performed with STN-DBS and midfrontal EEG. One block of 40 trials was performed at each DBS setting [high frequency (HF)-DBS and 4-Hz DBS]. Trials were presented in pseudorandom order. Participants were asked not to count in their head during the task. At least 30 min elapsed between DBS setting changes and task performance (Cooper *et al.*, 2013). All testing outside the operating room was done while patients took levodopa and other medications as usual. Levodopa does not reliably affect interval timing performance or midfrontal delta/theta rhythms (Parker *et al.*, 2015). Only seven patients completed blocks with 4-Hz DBS stimulation, 10 patients completed the other blocks. No patients or blocks were excluded. All STN-DBS patients were stable on medications and DBS for at least 1 month, and all had implants at least 3 months prior to testing. Response times were analysed using a linear mixed-effects model using reaction time as the dependent variable, DBS setting (typical HF-DBS, 4 Hz, or off) and interval (FI3 versus FI12) as fixed effects, and patients as random effects.

Human electrocorticography

Intracortical ECoG electrodes were referenced to an extracranial subgaleal electrode near the vertex. The ECoG signals were band-pass filtered (1.6–1000 Hz, −12 dB/octave anti-aliasing filter) and then digitized with a sampling frequency of 2034.5 Hz. Recordings from grid electrodes were inspected to ensure they were not contaminated by epileptiform activity or artefact and power-line noise was removed using an adaptive notch-filtering procedure. Patients with medial prefrontal coverage had depth electrodes that used ∼5 mm centre-to-centre spacing. The exact position of the recording arrays differed somewhat between patients as placement was based on patient-specific clinical considerations. In these patients, coverage included significant portions of medial prefrontal cortex. The electrodes remained in place during a 14-day hospital stay during which the patients underwent continuous video-EEG monitoring. EEG monitoring confirmed that the cortical areas pertinent to this study did not show abnormal interictal activity. None of these areas were part of the epileptogenic focus and its eventual resection. Experiments were conducted in a specially designed and electromagnetically-shielded private patient suite. Patients did not incur any additional medical or surgical risks by participating in this study.

Human electrical stimulation-functional MRI

All neurosurgical patients had detailed 3 T structural MRIs. These were used for indirect targeting of STN, diffusion tensor imaging (DTI), and electrode reconstruction. The reconstruction of the intracranial electrode contacts was performed using a combination of high-resolution digital photographs, and thin-cut pre- and post-implantation structural MRI ($1.0 \times 1.0 \times 1.0$ mm voxel size) and CT ($0.45 \times 0.45 \times 1.0$ mm voxel size) scans. Pre- and post-implantation CTs and MRIs were co-registered using a 3D rigid-fusion algorithm implemented in FMRIB's Linear Image Registration Tool (Jenkinson *et al.*, 2002). Coordinates for each electrode obtained from post-implantation MRI volumes were transferred to pre-implantation MRI volumes. The location of every contact relative to visible surrounding brain structures was compared in both pre- and post-implantation MRI volumes. The resultant electrode locations were then mapped to a 3D cortical surface rendering. The estimated overall error in electrode localization using these techniques does not exceed 2 mm based on visual inspection. Electrical stimulation-functional MRI was performed in two patients with medial PFC ECoG electrode coverage. Briefly, T_2*-weighted images (gradient echo-EPI) were acquired while electrical stimulus was delivered to the intracranial contacts. The stimulation was in bipolar fashion using adjacent depth electrode contacts. We used a 3 T MRI scanner (Siemens Trio). Charge-balanced square waves at 100 Hz and 9 mA current were delivered for midcingulate contacts. Blood oxygen level-dependent (BOLD) images were realigned, smoothed with a Gaussian kernel of 6 mm full-width at half-maximum, and analysed using a general linear model according to Oya *et al.* (2017).

EEG recording and analysis

In the operating room, a highly limited montage was used to acquire data with midfrontal EEG (∼AFz/Fz leads, depending on sterile field, frame placement, and other hardware, as well as ∼C3, ∼C4, and mastoids). For STN-DBS with EEG, recording and analysis was similar to methods described in detail previously (Narayanan *et al.*, 2013*a*; Parker *et al.*, 2015). EEG was recorded on a Biopac system with a sampling rate of 500 Hz. EEG was recorded from a 64-channel system. Impedance of all electrodes was below 5 kΩ. Continuous data were parsed into 16-s epochs (−2 to 14 s following the cue) and re-referenced to the mathematical average of the two mastoid channels, yielding a total of 62 scalp EEG channels. Eye blinks and horizontal eye movements were removed by hand using independent component analysis and the EEGLab MATLAB toolbox (Delorme and Makeig, 2004).

Subthalamic nucleus recording

STN-DBS implantation is staged such that bilateral DBS electrodes are implanted sequentially during a single stereotactic procedure. Prior to surgery, midfrontal and reference EEG electrodes are placed. We elected to compare STN activity to midfrontal EEG electrodes because (i) it was technically more feasible than inserting an ECoG strip though the DBS burr hole as described above; and (ii) delta/theta oscillations from midfrontal EEG electrodes in patients with Parkinson's disease have been well described by our group and others (Narayanan *et al.*, 2013*a*; Cavanagh and Frank, 2014; Parker *et al.*, 2015; Chen *et al.*, 2016). Patients underwent standard bilateral DBS implantation via indirect framed stereotactic targeting of the STN refined by multielectrode recordings from 0.4 to 0.8 mΩ tungsten electrodes (Alpha-Omega). Three to five microelectrode recording tracks were used, consisting of anterior, middle, and posterior microelectrode recording trajectories at ∼74° from the horizontal separated by 2 mm centre-to-centre. STN margins are defined by preoperative anatomy as well as the functional and electrical properties from STN

microelectrode recording. All interval timing task stimuli were auditory and were delivered via headphones. Behavioural and neurophysiological data were acquired simultaneously using a Tucker-Davis Technologies multi-channel system. Microelectrode recording was sampled at 24 kHz, amplified, and filtered for single neurons (1–8 kHz) and STN LFPs (<200 Hz). Mastoid and subgaleal electrodes were used as references. Because microelectrode recording recordings are clinically necessary, patients were not exposed to extra electrode penetrations. With our intraoperative team, these experiments typically prolonged DBS surgery by <10 min/task, including set-up time. Patients did receive pain relief and sedative medications in the operating room; these were short-acting agents (e.g. remifentanil, dexmedetomidine), which were stopped >1 h prior to microelectrode recording in all 10 patients, allowing patients to be maximally awake for necessary clinical testing and participation in research. All electrodes were localized in the STN region by mapping individual intraoperative stereotactic coordinates to MNI space (Supplementary Fig. 1).

Neurophysiological analyses

Raw voltage from STN microelectrode recording was digitized at 24 kHz and filtered at <200 Hz for LFP and 0.3–8 kHz for neurons. Spike detection was performed by thresholding using a median absolute deviation of 4. Spikes were pre-sorted using unsupervised wavelet-based clustering and then sorted manually using principal component analyses (PCA) in Plexon's offline sorter according to procedures outlined at length previously (Laubach *et al.*, 2015; Parker *et al.*, 2015). Spike activity was analysed for all cells that fired at rates above 0.1 Hz. PCA and waveform shape were used for spike sorting. Single units were identified as having (i) consistent waveform shape; (ii) separable clusters in PCA space; and (iii) a consistent refractory period of at least 2 ms in interspike interval histograms. Significant cue- and response-related modulation was defined as neurons with a significant difference in mean firing-rate 1 s before and after events via a paired *t*-test. We defined time-related ramping activity as firing rate that progressed linearly over the interval according to the formula:

$$y = at + c \quad (1)$$

where y is firing rate, t is the time in seconds, and a is the slope.

Time-frequency and neuronal analyses

Time-frequency calculations were computed using custom-written MATLAB routines according to the methods described at length previously (Cavanagh *et al.*, 2009). Time-frequency measures were computed by multiplying the fast-Fourier transformed (FFT) power spectrum of LFP data with the FFT power spectrum of a set of complex Morlet wavelets [defined as a Gaussian-windowed complex sine wave: $e^{i2\pi tf}e^{-\frac{t^2}{2\times\sigma^2}}$, where t is time, f is frequency (which increased from 1 to 50 Hz in 50 logarithmically spaced steps), and defines the width (or 'cycles') of each frequency band, set according to 4/[2πf], and taking the inverse FFT. The end result of this process is identical to time-domain signal convolution, and it resulted in: (i) estimates of instantaneous power (the magnitude of the analytic signal), defined as Z[t] {power time series: $p(t) = real[z(t)]^2 + imag[z(t)]^2$}; and (ii) phase (the phase angle) defined as = arctan (imag[z(t)]/real[z(t)]). Each epoch was then cut in length surrounding the event of interest (−1500 to +2000 ms around the event). Power was normalized by conversion to a decibel (dB) scale {10 × log10[power(t)/power(baseline)]} from a prestimulus baseline of −500 to −300 ms, allowing a direct comparison of effects across frequency bands. To quantify time-frequency components of interactions between individual spikes and the field potential, we applied field-field coherence and spike-field coherence analysis using the Neurospec toolbox (Rosenberg *et al.*, 1989; Narayanan *et al.*, 2013*a*; Parker *et al.*, 2014), in which multivariate Fourier analysis was used to extract phase-locking among spike trains and LFPs. Phase-locking coherence values varied from 0 to 1, where 0 indicates no coherence and 1 indicates perfect coherence. To compare across neurons with different distributions, all phase-locking values were divided by the 95% confidence for each interval, so that 1 indicates a $P < 0.05$. To examine how DBS affected medial PFC, we analysed a region of interest of midfrontal EEG contacts. Our hypothesis related to low-frequency PFC-STN connectivity was shaped by extensive prior work pertaining to cue-triggered delta rhythms at 1–4 Hz 300–500 ms after cue onset at midfrontal region of interest (Ridderinkhof *et al.*, 2004; Narayanan *et al.*, 2013*a*; Cavanagh and Frank, 2014; Parker *et al.*, 2014, 2015, 2017). Notably, we did not observe any effects of DBS outside this region. As in our behavioural analyses, we used a linear mixed-effects model in which the dependent variable was response times, fixed effects were mean cue-triggered midfrontal power (1–4 Hz, 300–500 ms after cue onset) and DBS setting, and random effects were electrode location and patients. For trial-by-trial analyses of midfrontal power on response time (RT), we also used a linear mixed-effects model [RT ~ Power × DBS + (1 | Subject); Supplementary Table 5].

Granger causality

Raw LFPs recorded at midfrontal EEG sites and STN were downsampled to 200 Hz and a 59–61 Hz Butterworth notch filter was applied to remove line noise (Barrett *et al.*, 2012). We selected a model order of 100 ms and 200 ms sliding-time segments (six segments per 12-s interval-timing trial) for subsequent analysis to maximize the resolution of low-frequency Granger prediction. A model order of 500 ms contains ⩾1 cycle of a ⩾ 2 Hz oscillation, allowing increased frequency specificity of Granger prediction. Because larger model order increases the risk of non-stationarity in time-series data, we subtracted single-patient event-related potentials from time-series segments, detrended, and z-scored all modelled data. Corrected time-series segments were submitted to KPSS unit root testing using MVGC Toolbox routines to determine single-trial KPSS test statistics. Statistical testing of stationarity was performed by compared single-trial KPSS test statistics to a non-stationarity critical value computed at $P = 0.05$. Significant Granger causality during 12-s interval timing was assessed using Granger's F-test routines in MVGC Toolbox at $P = 0.05$. Inputs were F-statistics from grand-averaged time segments for directed connectivity between middle frontal cortex (MFC) and STN in experimental and time-shuffled data. To visualize band-limited directed connectivity, *armorf.m*-derived autoregression coefficient matrices were Fourier-transformed and inverted to generate transfer

functions for the spectral factorization of autoregression residuals. Spectral pairwise Granger prediction was subsequently calculated by inverse-Fourier transformation of spectral factorization outputs, resulting in time-frequency domain connectivity estimates (Barnett and Seth, 2014; Cohen, 2014).

Results

Hyperdirect connections between frontal cortex and the STN have not been previously established in humans, although indirect techniques such as DTI and functional brain imaging have described frontal-STN connectivity (Brunenberg *et al.*, 2012; Haynes and Haber, 2013; Averbeck *et al.*, 2014). We used ESTT experiments during DBS implantation surgery to investigate STN connectivity. This technique involves single-pulse brain stimulation and recording of evoked responses in functionally-connected sites in PFC (Greenlee *et al.*, 2004). We performed STN stimulation via stereotactically-implanted DBS electrodes and recorded evoked responses from subdural ECoG electrodes located over primary motor cortex and the middle frontal gyrus of lateral PFC (Fig. 1A, B and Supplementary Figs 1 and 2). STN stimulation evoked short-latency lateral PFC and motor cortical responses (~12 ms), consistent with hyperdirect lateral PFC–STN functional connectivity (Fig. 1B and C; $P < 0.01$, see also Supplementary Table 1). PFC ECoG sites are ~9 cm away from the STN, and cortical white matter conducts at ~7–10 m/s; latencies between 9–13 ms might be expected if STN current depolarized and backfired axons of PFC neurons, resulting in antidromic stimulation (Swadlow and Waxman, 1976; Mathai and Smith, 2011). Cortical responses were ipsilateral, stimulation voltage-dependent, and observed in 5/5 patients with 10 V STN stimulation (Fig. 1C, Supplementary Fig. 5 and Supplementary Tables 1–3). In line with prior studies in non-human primates, brain imaging studies in humans, and models of hyperdirect function (Nambu *et al.*, 2002; Haynes and Haber, 2013; Averbeck *et al.*, 2014; Alkemade *et al.*, 2015), these results are consistent with monosynaptic projections from the lateral PFC and motor cortex to the STN in humans.

DBS implantation tracks for clinically-indicated neurosurgical procedures are proximate to lateral PFC sites in middle frontal gyrus. However, these tracks are distant from medial areas of PFC (medial PFC) such as anterior cingulate that are critically involved in cognitive control. Consequently, it is difficult to record from medial PFC with ESTT while stimulating the STN in humans (Ridderinkhof *et al.*, 2004). On rare occasions, epilepsy patients have depth electrode arrays implanted in medial PFC as part of epilepsy surgical evaluations (Supplementary Table 2). These patients therefore present an opportunity to explore STN connectivity with medial PFC. We performed electrical stimulation of medial PFC contacts and measured BOLD functional MRI responses (electrical stimulation-functional MRI) evoked by the stimulation in patients with depth electrodes in the medial PFC. Similar to ESTT, electrical stimulation-functional MRI also captures monosynaptic connections (Logothetis *et al.*, 2010; Logothetis, 2012; Oya *et al.*, 2017). We stimulated midcingulate medial PFC contacts and identified BOLD signal within the STN region (Fig. 2A, B and Supplementary Fig. 6). In concert with the ESTT data above as well as prior tract-tracing and neuroimaging data, these results provide direct evidence of hyperdirect connectivity between the PFC and STN (Brunenberg *et al.*, 2012; Haynes and Haber, 2013; Averbeck *et al.*, 2014; Alkemade *et al.*, 2015).

We studied the significance of medial PFC and STN connectivity by directly recording from both areas during performance of an elementary cognitive task: interval timing.

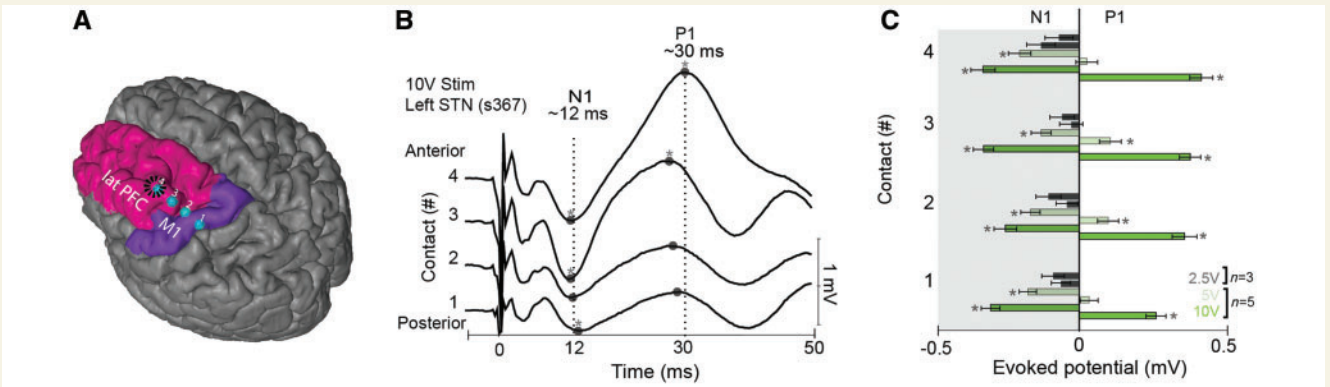

Figure 1 Novel functional connectivity between frontal cortex and STN in humans. (**A**) Lateral PFC (lPFC; contacts 3–4) and motor sites (contacts 1–2) were accessed by a four-electrode strip placed via burr hole (outlined in black) in human patients undergoing STN-DBS. (**B**) Stimulating the STN resulted in short-latency transients (N1) at ~12 ms. The latencies of these transients are consistent with back-propagating antidromic activity originating from STN. Longer latency positive peaks (P1) at ~30 ms were also observed. (**C**) N1/P1 amplitudes at lateral PFC as a function of STN stimulation strength (10 V and 5 V) in five patients; 2.5-V stimulation was performed in three patients. See also Supplementary Fig. 1 and 2.

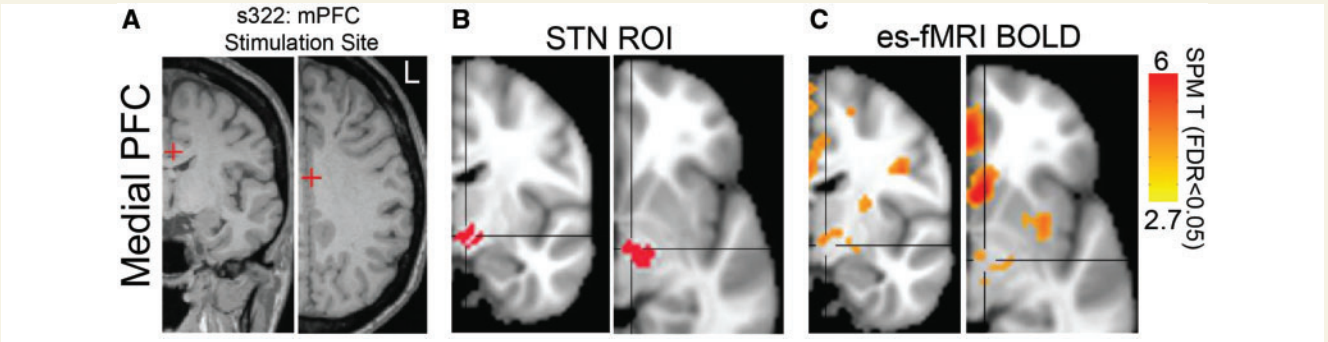

Figure 2 Novel functional connectivity between medial PFC and STN in humans. (**A**) We also studied connectivity between medial PFC (mPFC) and STN using electrical stimulation-functional MRI (es-fMRI), which reveals functional connectivity from a stimulated site in mid-cingulate cortex. (**B** and **C**) Electrical stimulation-functional MRI BOLD signal was seen in areas with known connectivity, including the STN (data from an exemplar patient; region of interest in red, BOLD in orange, FDR $P < 0.05$). See also Supplementary Fig. 3.

This task requires patients to make a motor response 3 or 12 s after a starting cue (Fig. 3A). Interval timing is ideal for intraoperative neurophysiology because (i) it has simple instructions and requires a single response; (ii) it is impaired in patients with Parkinson's disease; and (iii) it involves executive functions such as working memory for temporal rules and attention to the passage of time (Parker *et al.*, 2013). Because interval timing involves highly conserved medial frontal circuitry across species, we focused on medial PFC for the remainder of this manuscript (Parker *et al.*, 2015, 2017; Kim *et al.*, 2017). During interval timing, patients with Parkinson's disease in surgery responded at 2.9 ± 0.3 s on 3 s (FI3) trials, and at 8.4 ± 1.2 s on 12 s (FI12) trials ($P < 0.0004$). FI3 and FI12 performance was similar inside versus outside the operating room, as previously reported (Cavanagh *et al.*, 2011) (Supplementary Fig. 4). By comparison, control patients had response times of 3.1 ± 0.1 s on FI3 trials versus 12.5 ± 0.3 s on FI12 trials (data from 13 demographically-matched controls in our prior work) (Parker *et al.*, 2015; Kim *et al.*, 2017).

We used two methods to study human medial PFC physiology during interval timing. First, we directly recorded from medial PFC using ECoG depth electrodes and found robust cue-related delta/theta oscillations between 1 and 8 Hz during interval timing (Fig. 3B and C). Second, we leveraged the fact that midfrontal scalp EEG electrodes (i.e. AFz, Fz, Cz) reflect medial PFC activity (Cavanagh and Frank, 2014). We observed cue-triggered delta/theta 1–4 Hz activity from midfrontal EEG leads in 10 patients with Parkinson's disease receiving STN-DBS implants (Fig. 3D). In these patients, we also found cue-modulated low-frequency activity in the STN (Fig. 3E and Supplementary Fig. 4) and identified strong ~4 Hz coherence between midfrontal EEG and STN (Fig. 3F). Such coherence may represent functional connectivity between medial PFC and STN but does not measure directionality. Therefore, we used Granger causality to examine effective connectivity between midfrontal EEG and STN at specific frequency bands (see 'Granger causality' section). Granger causality analyses revealed that midfrontal EEG causally led STN signals at ~4 Hz (versus shuffled data: $P < 0.002$; STN → midfrontal EEG: $P < 0.02$; Fig. 3G). Similar patterns of low-frequency coherence and causality were seen around the time of response (Supplementary Fig. 4). As in past work, we also noted ~12–25-Hz beta coherence and causality around response (de Hemptinne *et al.*, 2013; Zavala *et al.*, 2013, 2014; Herz *et al.*, 2016). Similar 4-Hz STN → midfrontal EEG connectivity has also been found during conflict tasks (Cavanagh *et al.*, 2011; Zavala *et al.*, 2014). Together, these findings demonstrate functional coupling of midfrontal EEG and STN at 4 Hz during elementary cognitive processing.

Recordings from single neurons can provide an additional window into detailed information processing by neural circuits beyond macro-level signals like EEG and LFPs (Narayanan *et al.*, 2013*a*). To further elucidate the relationship between PFC and STN during interval timing, we recorded single-unit neuronal activity in the STN during interval timing with high-impedance microelectrodes used during DBS implantation surgery (Supplementary Fig. 5). Significant modulation around task events was observed in 24 of 36 well-isolated STN neurons (67%). Six were significantly cue modulated (17%; Fig. 4A and Supplementary Fig. 6) and 18 were response modulated (50%; Fig. 4B and Supplementary Fig. 6).

Midfrontal EEG recordings from Fig. 3 indicated that medial PFC can synchronize STN LFPs at 4 Hz. Past work has shown that medial PFC delta/theta activity is a prominent cognitive control signal modulated after errors, conflict, or cognitively salient events (Cavanagh and Frank, 2014) and that it engages single neurons in distant brain areas to promote goal-directed behaviour. Surprisingly, we found that cue-related STN neurons had ~4-Hz spike-field coherence with midfrontal EEG ($P < 0.04$; Fig. 4C). This pattern was not observed for response-modulated STN neurons (Fig. 4D) or for STN field/STN neuron coherence (Supplementary Fig. 5). STN neurons could also encode

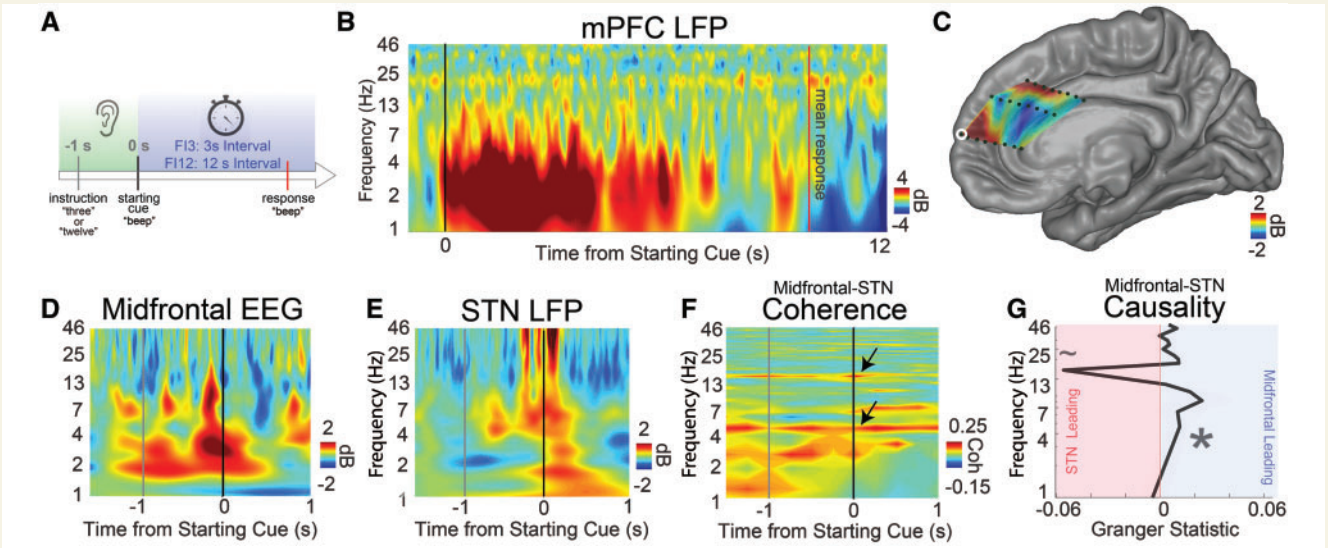

Figure 3 During cognitive processing, 4-Hz medial PFC signals exert top-down control of the STN. (**A**) We used interval timing tasks to study elementary cognitive processing in PFC and STN. During interval timing, patients heard an instruction telling them how long to wait (3 or 12 s), then a starting cue indicating that they should start timing. Patients reported their estimate of the interval by making a button-press response. (**B**) We recorded LFPs from depth electrodes in human medial PFC (mPFC), which has been implicated in interval timing across species. Time-frequency analysis revealed robust cue-triggered low-frequency delta/theta activity between 1 and 8 Hz in medial PFC. (**C**) The amount of 1–4 Hz activity at 300–500 ms post-cue was interpolated across medial PFC depth electrodes, showing cue-triggered modulation at dorsal medial PFC and rostral and middle cingulate gyri. (Contact from **B** outlined in white.) (**D** and **E**) We collected human intraoperative data from 10 patients with Parkinson's disease undergoing STN-DBS implantation performing the interval timing task. Time-frequency analyses revealed cue-triggered delta/theta activity from intraoperative midfrontal EEG (~AFz/Fz) and STN during cues. (**F**) Midfrontal EEG and STN had strong, task-independent coherence at ~4 Hz and at ~20 Hz in the beta range (arrows; raw coherence >0.17 is significant at 95% CI). (**G**) Granger causality analyses around the cue revealed that at 4 Hz, midfrontal EEG oscillations led the STN while ~20-Hz STN oscillations led midfrontal EEG. Ten patients with Parkinson's disease undergoing STN-DBS implantation. *$P < 0.05$; ~$P < 0.10$. All data from FI12 trials. See also Supplementary Fig. 4.

temporal aspects of interval-timing tasks (Supplementary Fig. 6) (Fujisawa and Buzsáki, 2011; Narayanan *et al.*, 2013*a*; Parker *et al.*, 2015; Karalis *et al.*, 2016). These data demonstrate that medial PFC delta/theta rhythms can engage single neurons as well as STN LFPs.

These data lead to the hypothesis that 4-Hz coherence between medial PFC-STN is critical for cognitive control during interval timing. We tested this prediction by stimulating the STN at 4 Hz in patients with Parkinson's disease implanted with STN-DBS systems while recording scalp EEG. Of note, high-frequency STN-DBS (HF-DBS) for clinical indications is set between 60 and 180 Hz to treat motor symptoms of Parkinson's disease (Follett *et al.*, 2010); lower frequencies at ~10 Hz can modulate timing task performance but typically worsen motor symptoms of Parkinson's disease (Barnikol *et al.*, 2008; Wojtecki *et al.*, 2011). To our knowledge, 4-Hz STN-DBS has never been explored in any setting. Patients performed interval-timing tasks in three DBS conditions: DBS off, HF-DBS (at the patient baseline/normal programmed settings; 120–150 Hz), and 4-Hz DBS. DBS amplitude, pulse width, and active contacts were not altered (Supplementary Table 1). As predicted, 4-Hz STN-DBS increased cue-related delta activity (1–4 Hz) at midfrontal EEG sites ($P < 0.00006$; Fig. 5A–F). Consistent with past work, trial-by-trial analyses using linear mixed-effects modelling demonstrated that both cue-triggered midfrontal delta power (1–4 Hz, 300–500 ms after cue onset) ($P < 0.02$) and DBS frequency ($P < 10^{-16}$) predicted response times in FI12 trials (Supplementary Table 5) (Cavanagh *et al.*, 2011; Parker *et al.*, 2015). No similar pattern was seen at midfrontal EEG around response (Supplementary Fig. 7).

Strikingly, 4-Hz STN-DBS improved Parkinson's disease subject performance on FI12 trials, bringing responses closer to 12 s and the response times of normal controls (Fig. 5G and H) (main effect of DBS $P < 0.04$; interaction of Interval × DBS $P < 0.004$). HF-DBS did not change interval timing performance compared to DBS off. These data suggest that 4-Hz STN-DBS can boost midfrontal cue-related 4-Hz activity and improve performance of interval-timing tasks by bringing responses in FI12 trials closer to 12 s. Crucially, there were no consistent effects at FI3, indicating that 4-Hz DBS did not merely slow motor responses. Patients with Parkinson's disease are most impaired on FI12 trials, likely due to the increased difficulty of maintaining temporal processing over durations as long as 12 s (Parker *et al.*, 2013). These findings are supported by previous studies showing that STN-DBS can modulate timing, decision thresholds and other cognitive signals in humans (Cavanagh *et al.*, 2011; Wessel *et al.*, 2016). When

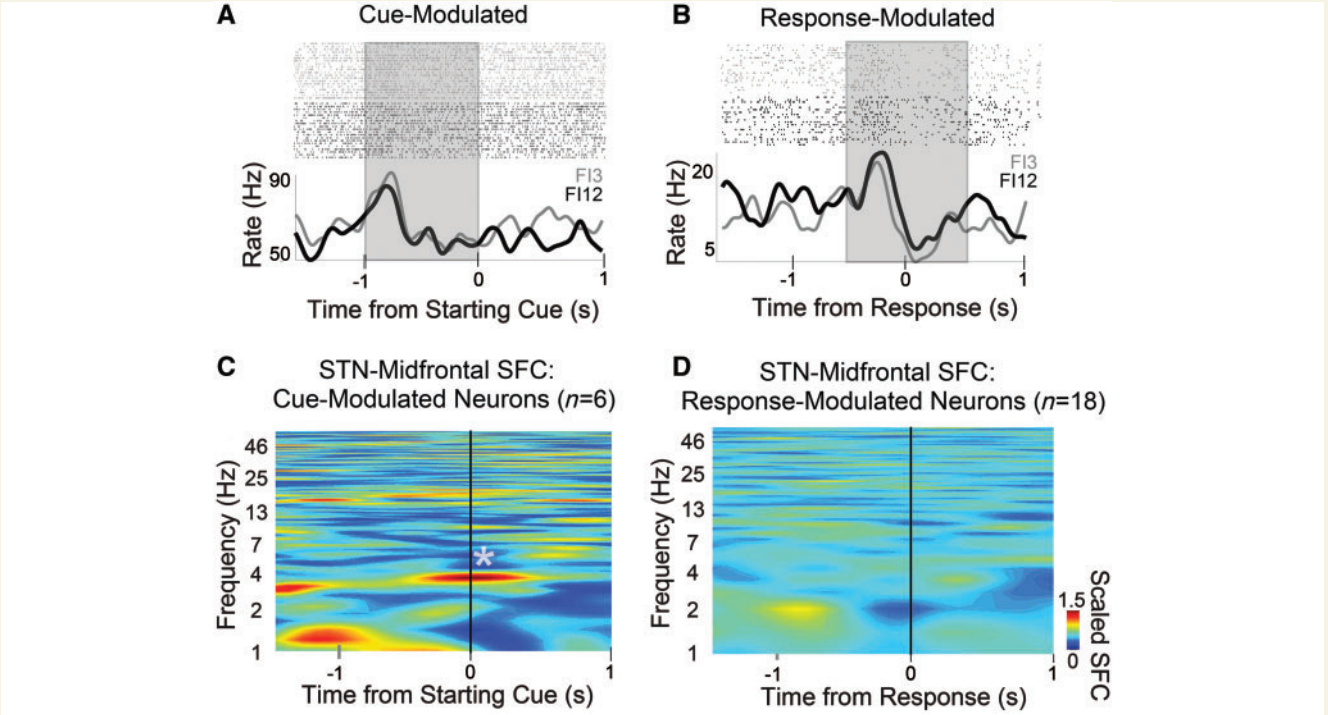

Figure 4 Medial PFC synchronizes human STN neurons at 4 Hz. (**A**) Peri-event rasters and histograms for human STN neurons during interval timing for FI3 (grey) and FI12 (black) trials aligned to cue onset ('three' or 'twelve'); this neuron was cue-modulated during the instruction period from −1 to 0 s (shaded area). (**B**) Response-modulated human STN neuron; shaded area used to calculate firing rate modulation. (**C**) Cue-modulated human STN neurons (n = 6) had significant 4-Hz spike-field coherence (SFC) with midfrontal EEG. (**D**) This pattern was not seen for response-modulated neurons.

integrated with our data on medial PFC-STN connectivity and STN neuronal activity, these findings demonstrate that medial PFC and the STN interact at 4 Hz to affect cognitive control.

Discussion

We leveraged human intraoperative neurophysiology to investigate human hyperdirect connections between PFC and STN. First, we showed that the STN appears to be physiologically connected to motor cortex and PFC. Second, we observed cue-evoked delta/theta activity and top-down functional coupling between medial PFC and STN during a cognitive task (interval-timing task). Third, we found that STN-DBS in that same frequency range improved cognitive performance in the interval-timing task. Typical STN-DBS protocols used to treat motor symptoms use high frequencies (>120 Hz). Here, we show that low-frequency stimulation (4 Hz) has the potential to modulate behavioural performance in tasks involving cognitive processing. Together, this work shows that low-frequency signalling along the hyperdirect pathway can modulate cognitive control in humans.

Our data provide the first direct evidence of a hyperdirect pathway between PFC and STN in humans. Notably, our data are primarily physiological rather than anatomical, and suggest a functional hyperdirect connection between PFC and STN. Combined with detailed non-human anatomical tracing studies (Nambu *et al.*, 2002; Haynes and Haber, 2013; Averbeck *et al.*, 2014), these data indicate that the STN may receive cognitive input from PFC as well as motor input from primary motor cortex. This overlap provides insight into cognitive processing in the STN and could help illuminate why STN-DBS has cognitive side effects in some patients.

Our clinical DBS targeted motor sites in the dorsolateral STN, which is classically designated a motor integration area. However, the STN is compact, and there is likely substantial overlap between its functional areas (Alkemade *et al.*, 2013, 2015; Alkemade and Forstmann, 2014). Non-human primate work shows that the STN clearly receives convergent input from PFC as well as motor cortex (Haynes and Haber, 2013; Alkemade *et al.*, 2015). Our ESTT and electrical stimulation-functional MRI data capture this frontal-STN connectivity in humans. Past work has described cognitive processing captured at motor STN sites (Zavala *et al.*, 2013, 2016; Herz *et al.*, 2016) and our results indicate that we can detect significant medial PFC-STN interactions in the motor STN (Haynes and Haber, 2013; Averbeck *et al.*, 2014; Alkemade *et al.*, 2015). This complex anatomy might help understand the cognitive side effects of STN DBS and could also lead to

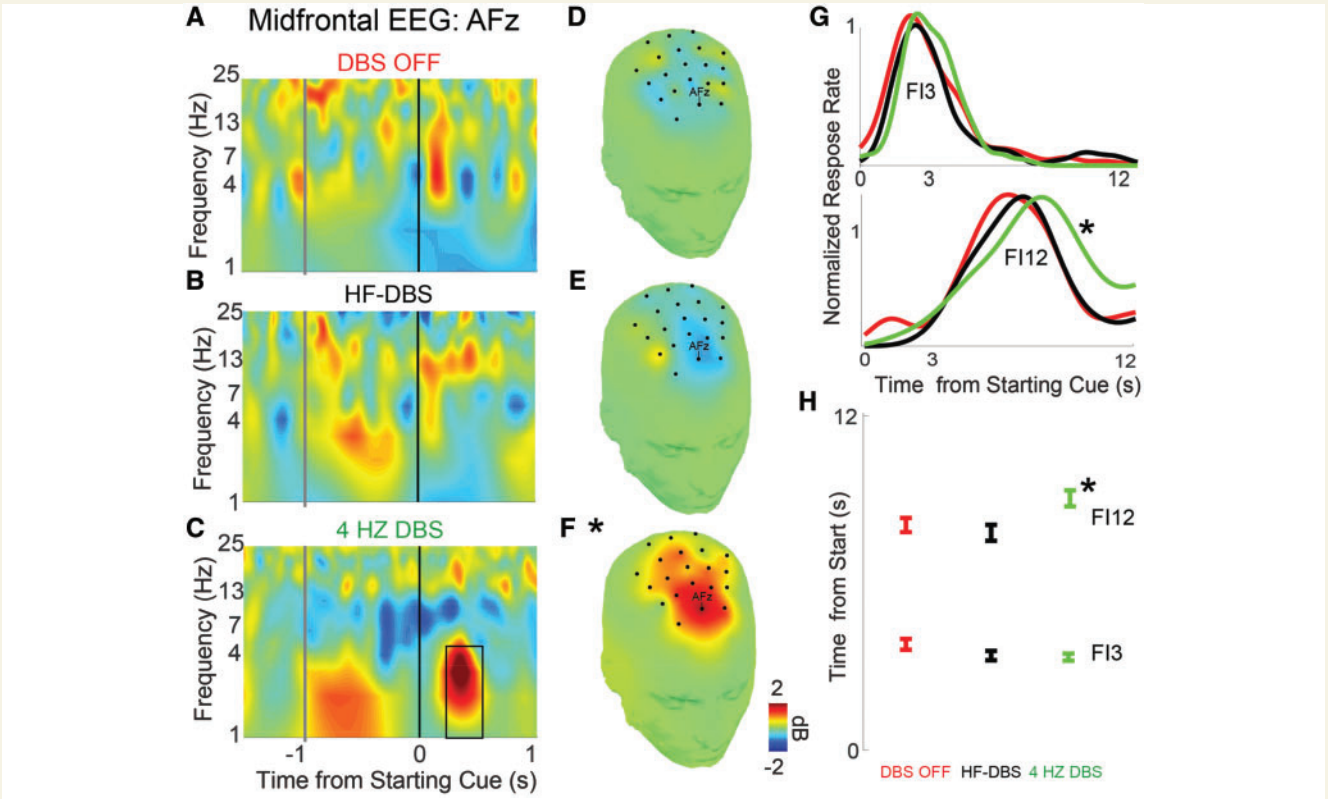

Figure 5 STN-DBS (4-Hz) improves interval timing performance. Time-frequency analysis of starting cue-related activity at midfrontal EEG contact AFz for (**A**) DBS off, (**B**) DBS at high frequencies (~130 Hz; HF-DBS) and (**C**) 4-Hz DBS. Black box represents the region of interest analysed by linear mixed-effect models over midfrontal EEG leads (1–4 Hz, 300–500 ms; $^*P < 0.05$). Topography of midfrontal delta power in this region of interest is shown for (**D**) DBS off, (**E**) HF-DBS and (**F**) 4-Hz DBS. (**G**) Distributions of response times on FI3 (*top*) and FI12 (*bottom*) trials for blocks with DBS OFF (red), HF-DBS (black), and at 4 Hz (green). (**H**) 4-Hz DBS improved performance of FI12 trials, but not FI3 trials. Data from 10 patients with STN-DBS, seven of whom had 4-Hz DBS blocks. Mean response time ± standard error of the mean across all trials in all patients. $^*P < 0.05$.

new therapies for diseases with impaired cognitive processing.

Prior work consistently implicates the STN in preventing premature responses and regulating decision thresholds (Baunez and Robbins, 1997; Aron and Poldrack, 2006; Frank, 2006; Aron *et al.*, 2007; Isoda and Hikosaka, 2008; Cavanagh *et al.*, 2011; Zavala *et al.*, 2014; Frank *et al.*, 2015; Herz *et al.*, 2017; Wessel and Aron, 2017). In the present study, we found that 4-Hz STN-DBS could delay responding in patients with Parkinson's disease on FI12 trials on which they are normally biased towards responding quickly. Thus, during interval timing 4-Hz STN-DBS may better engage medial PFC-STN circuits (relative to 130-Hz STN-DBS, or DBS off) and thus improve the ability to inhibit impulsive/premature responses. There was no effect of 4-Hz STN-DBS on FI3 trials for patients with Parkinson's disease; of note, on these trials, patients with Parkinson's disease did not have marked behavioural deficits to begin with (Parker *et al.*, 2015; Kim *et al.*, 2017). These data are largely consistent with the STN's role in decision thresholds, but much work needs to be done to extend our findings beyond interval timing.

The hyperdirect pathway has previously been shown to couple motor cortex and STN at beta-range frequencies to facilitate motor control (Nambu *et al.*, 2002; Zaghloul *et al.*, 2012; de Hemptinne *et al.*, 2015). Additionally, we found evidence of 4-Hz interactions. Our findings are consistent with prior reports that STN neurons and 4-Hz STN LFP activity are involved in conflict and flanker tasks (Zaghloul *et al.*, 2012; Zavala *et al.*, 2013; Herz *et al.*, 2016). During such tasks, increased delta/theta coherence (1–8 Hz) in the STN can be seen at moments requiring cognitive control, such as after errors or on high-conflict trials (Zavala *et al.*, 2014, 2016). Medial PFC rhythms (4 Hz) have been advanced as a cognitive control signal that is modulated at critical moments when such control is required (Narayanan *et al.*, 2013*a*; Cavanagh and Frank, 2014). We extend this line of research to show that medial PFC 4-Hz rhythms may be responsible for synchronizing STN LFPs and engaging cue-modulated STN single neurons.

Our working model is that medial PFC delta/theta rhythms actively engage cognitive control processes, including single neurons explicitly involved in temporal

processing (Narayanan *et al.*, 2013*a*; Cavanagh and Frank, 2014; Parker *et al.*, 2014). These cognitive control processes are initiated by the starting cue of an interval timing task, triggering working memory for temporal rules and attention to the passage of time (Church, 2003; Parker *et al.*, 2013). FI3 trials place a smaller demand on working memory/attention. Thus, the 3-s interval engages less cognitive control than the 12-s interval. Our patients with Parkinson's disease have minimal impairments in FI3 trials and HF-DBS produces fewer deficits. However, on FI12 trials, more cognitive control is required to recruit working memory/attentional processes; these processes are impaired in patients with Parkinson's disease resulting in impaired timing performance. According to this model, 4-Hz STN-DBS modulates medial PFC delta/theta activity and increases cognitive control. Future studies of 4-Hz STN DBS in tasks requiring additional cognitive control will further test our model.

Delta/theta rhythms are impaired in patients with Parkinson's disease and in animal models with depleted dopamine (Parker *et al.*, 2015; Chen *et al.*, 2016; Kim *et al.*, 2017), although we note that the high-functioning patients with Parkinson's disease who qualified for STN-DBS in this study had some residual delta/theta activity. Thus, this frequency band is ripe for exploration of invasive and non-invasive brain stimulation aimed at boosting cognitive control. Our past work indicated that stimulation in this range could compensate for deficits in interval timing caused by prefrontal dopamine disruption in rodent models (Kim *et al.*, 2017; Parker *et al.*, 2017). In this study, we found in humans that 4-Hz STN-DBS can improve performance of an interval timing task. These data are of particular significance because cognitive impairment is common in Parkinson's disease. Furthermore, patients with STN-DBS may have cognitive decline exacerbated by high-frequency STN-DBS (Heo *et al.*, 2008; Okun *et al.*, 2009).

We focus on interval timing because it is a cognitive process that is reliably impaired in Parkinson's disease and involves delta/theta medial PFC rhythms (Malapani and Rakitin, 2003; Parker *et al.*, 2013, 2015; Kim *et al.*, 2017). High-functioning Parkinson's disease patients who are DBS candidates can also have impairments during conflict, flanker, and stop-signal tasks, but have rather inconsistent impairments on other tests of executive function (Narayanan *et al.*, 2013*b*). Conflict and flanker tasks also involve delta/theta medial PFC activity (Cavanagh and Frank, 2014), but it has yet to be established whether patients with Parkinson's disease have delta/theta impairments in these tasks. These tasks are significantly more difficult to execute in the complex intraoperative environment. Our work here is confined to interval timing tasks that we have studied extensively in humans and rodents in the context of prefrontal dopamine (Narayanan *et al.*, 2012; Parker *et al.*, 2013, 2015, 2017; Kim *et al.*, 2017). Future work will be required to establish the scope of delta/theta hyperdirect medial PFC-STN interactions in other contexts, and to test whether the effects of 4-Hz STN-DBS generalizes to other cognitive tasks or real-world cognitive function.

Our approach has technical limitations related to working with human patients. Human intraoperative neurophysiology is conducted in patients with advanced Parkinson's disease who are off their usual medications and in a complex intraoperative environment. Intracranial electrode locations in epilepsy patients were dictated by clinical constraints; thus, our anatomical coverage is often incomplete and only rarely samples the subregions of PFC that we are most interested in. We are not aware of prior lateral PFC ECoG recordings during interval timing tasks. Technical limitations of combining ECoG, ESTT, and intracranial recordings during interval timing impeded our ability to record from lateral PFC in this study. Because ~4-Hz signals are a cognitive control signal across frontal cortex (Harmony, 2013; Cavanagh and Frank, 2014; Kingyon *et al.*, 2015), we predict that there would also be strong delta/theta lateral PFC-STN interactions.

Notably, STN-DBS at low frequencies does not improve and may worsen motor symptoms of Parkinson's disease (Barnikol *et al.*, 2008); thus, alternative DBS strategies are likely needed to clinically target both motor and cognitive function. We also cannot be sure if the effects boosting behaviour are due to antidromic excitation of the hyperdirect pathway, feed-forward excitation, or other effects of 4-Hz STN-DBS. Still, our data are clear that there are functional PFC-STN interactions at 4 Hz that instantiate cognitive control.

In summary, we elucidated hyperdirect cortico-subthalamic interactions in humans. In particular, STN LFPs and single neurons were coherent with 4-Hz medial PFC rhythms associated with cognitive control. Additionally, STN-DBS at 4 Hz improved cognitive performance in an interval timing task. Our work indicates that it may be possible to stimulate the STN at low frequencies to treat cognitive symptoms of Parkinson's disease and other human diseases.

Acknowledgements

We would like to thank Haiming Chen for technical assistance, as well as Michael J. Welsh and Michael A. Long for feedback on this manuscript.

Funding

This work was supported by National Institute of Neurological Disorders and Stroke Grants R01 NS089470, and National Institute of General Medical Sciences Grant NIH T32 GM007337 to the Medical Scientist Training Program at the University of Iowa Carver College of Medicine.

Supplementary material

Supplementary material is available at Brain online.

References

Alexander GE, Crutcher MD. Functional architecture of basal ganglia circuits: neural substrates of parallel processing. Trends Neurosci 1990; 13: 266–71.

Alkemade A, Forstmann BU. Do we need to revise the tripartite subdivision hypothesis of the human subthalamic nucleus (STN)? Neuroimage 2014; 95: 326–9.

Alkemade A, Keuken MC, Forstmann BU. A perspective on terra incognita: uncovering the neuroanatomy of the human subcortex. Front Neuroanat 2013; 7: 40.

Alkemade A, Schnitzler A, Forstmann BU. Topographic organization of the human and non-human primate subthalamic nucleus. Brain Struct Funct 2015; 220: 3075–86.

Aron AR, Behrens TE, Smith S, Frank MJ, Poldrack RA. Triangulating a cognitive control network using diffusion-weighted magnetic resonance imaging (MRI) and functional MRI. J Neurosci 2007; 27: 3743–52.

Aron AR, Poldrack RA. Cortical and subcortical contributions to Stop signal response inhibition: role of the subthalamic nucleus. J Neurosci 2006; 26: 2424–33.

Averbeck BB, Lehman J, Jacobson M, Haber SN. Estimates of projection overlap and zones of convergence within frontal-striatal circuits. J Neurosci 2014; 34: 9497–505.

Barnett L, Seth AK. The MVGC multivariate Granger causality toolbox: a new approach to Granger-causal inference. J Neurosci Methods 2014; 223: 50–68.

Barnikol UB, Popovych OV, Hauptmann C, Sturm V, Freund H-J, Tass PA. Tremor entrainment by patterned low-frequency stimulation. Philos Trans R Soc Lond Math Phys Eng Sci 2008; 366: 3545–73.

Barrett AB, Murphy M, Bruno M-A, Noirhomme Q, Boly M, Laureys S, et al. Granger causality analysis of steady-state electroencephalographic signals during propofol-induced anaesthesia. PLoS One 2012; 7: e29072.

Baunez C, Robbins TW. Bilateral lesions of the subthalamic nucleus induce multiple deficits in an attentional task in rats. Eur J Neurosci 1997; 9: 2086–99.

Benabid AL, Chabardes S, Mitrofanis J, Pollak P. Deep brain stimulation of the subthalamic nucleus for the treatment of Parkinson's disease. Lancet Neurol 2009; 8: 67–81.

Brunenberg EJL, Moeskops P, Backes WH, Pollo C, Cammoun L, Vilanova A, et al. Structural and resting state functional connectivity of the subthalamic nucleus: identification of motor STN parts and the hyperdirect pathway. PLoS One 2012; 7: e39061.

Caetano MS, Church RM. A comparison of responses and stimuli as time markers. Behav Processes 2009; 81: 298–302.

Cavanagh JF, Cohen MX, Allen JJB. Prelude to and resolution of an error: EEG phase synchrony reveals cognitive control dynamics during action monitoring. J Neurosci 2009; 29: 98–105.

Cavanagh JF, Frank MJ. Frontal theta as a mechanism for cognitive control. Trends Cogn Sci 2014; 18: 414–21.

Cavanagh JF, Wiecki TV, Cohen MX, Figueroa CM, Samanta J, Sherman SJ, et al. Subthalamic nucleus stimulation reverses mediofrontal influence over decision threshold. Nat Neurosci 2011; 14: 1462–7.

Chen K-H, Okerstrom KL, Kingyon JR, Anderson SW, Cavanagh JF, Narayanan NS. Startle habituation and midfrontal theta activity in Parkinson's disease. J Cogn Neurosci 2016: 1–11.

Chiken S, Nambu A. Disrupting neuronal transmission: mechanism of DBS? Front Syst Neurosci 2014; 8: 33.

Church R. A concise introduction to scalar timing theory [Internet]. In: Meck WH, editor. Functional and Neural Mechanisms of Interval Timing. Boca Raton, Florida: CRC Press; 2003. Available from: http://www.crcnetbase.com/doi/abs/10.1201/9780203009574.sec1 [24 July 2013, date last accessed].

Cohen MX. Analyzing neural time series data: theory and practice (Issues in clinical and cognitive neuropsychology). Cambridge, Massachusetts: The MIT Press; 2014.

Cooper SE, McIntyre CC, Fernandez HH, Vitek JL. Association of deep brain stimulation washout effects with Parkinson disease duration. JAMA Neurol 2013; 70: 95–9.

Delorme A, Makeig S. EEGLAB: an open source toolbox for analysis of single-trial EEG dynamics including independent component analysis. J Neurosci. Methods 2004; 134: 9–21.

Follett KA. Comparison of pallidal and subthalamic deep brain stimulation for the treatment of levodopa-induced dyskinesias [Internet]. Neurosurg Focus 2004; 17: E3. Available from: http://www.hubmed.org/display.cgi?uids=15264772

Follett KA, Weaver FM, Stern M, Hur K, Harris CL, Luo P, et al. Pallidal versus subthalamic deep-brain stimulation for Parkinson's disease. N Engl J Med 2010; 362: 2077–91.

Frank MJ. Hold your horses: a dynamic computational role for the subthalamic nucleus in decision making. Neural Netw 2006; 19: 1120–36.

Frank MJ, Gagne C, Nyhus E, Masters S, Wiecki TV, Cavanagh JF, et al. fMRI and EEG predictors of dynamic decision parameters during human reinforcement learning. J Neurosci 2015; 35: 485–94.

Fujisawa S, Buzsáki G. A 4 Hz oscillation adaptively synchronizes prefrontal, VTA, and hippocampal activities. Neuron 2011; 72: 153–65.

Gradinaru V, Mogri M, Thompson KR, Henderson JM, Deisseroth K. Optical deconstruction of parkinsonian neural circuitry. Science 2009; 324: 354–9.

Greenlee JDW, Oya H, Kawasaki H, Volkov IO, Kaufman OP, Kovach C, et al. A functional connection between inferior frontal gyrus and orofacial motor cortex in human. J Neurophysiol 2004; 92: 1153–64.

Harmony T. The functional significance of delta oscillations in cognitive processing. Front Integr Neurosci 2013; 7: 83.

Haynes WIA, Haber SN. The organization of prefrontal-subthalamic inputs in primates provides an anatomical substrate for both functional specificity and integration: implications for Basal Ganglia models and deep brain stimulation. J Neurosci 2013; 33: 4804–14.

de Hemptinne C, Ryapolova-Webb ES, Air EL, Garcia PA, Miller KJ, Ojemann JG, et al. Exaggerated phase-amplitude coupling in the primary motor cortex in Parkinson disease. Proc Natl Acad Sci USA 2013; 110: 4780–5.

de Hemptinne C, Swann NC, Ostrem JL, Ryapolova-Webb ES, San Luciano M, Galifianakis NB, et al. Therapeutic deep brain stimulation reduces cortical phase-amplitude coupling in Parkinson's disease. Nat Neurosci 2015; 18: 779–86.

Heo J-H, Lee K-M, Paek SH, Kim M-J, Lee J-Y, Kim J-Y, et al. The effects of bilateral subthalamic nucleus deep brain stimulation (STN DBS) on cognition in Parkinson disease. J Neurol Sci 2008; 273: 19–24.

Herz DM, Tan H, Brittain J-S, Fischer P, Cheeran B, Green AL, et al. Distinct mechanisms mediate speed-accuracy adjustments in cortico-subthalamic networks. eLife 2017; 6

Herz DM, Zavala BA, Bogacz R, Brown P. Neural correlates of decision thresholds in the human subthalamic nucleus. Curr Biol 2016; 26: 916–20.

Isoda M, Hikosaka O. Role for subthalamic nucleus neurons in switching from automatic to controlled eye movement. J Neurosci 2008; 28: 7209–18.

Jahfari S, Verbruggen F, Frank MJ, Waldorp LJ, Colzato L, Ridderinkhof KR, et al. How preparation changes the need for top-down control of the basal ganglia when inhibiting premature actions. J Neurosci 2012; 32: 10870–8.

Jenkinson M, Bannister P, Brady M, Smith S. Improved optimization for the robust and accurate linear registration and motion correction of brain images. Neuroimage 2002; 17: 825–41.

Karalis N, Dejean C, Chaudun F, Khoder S, Rozeske RR, Wurtz H, et al. 4-Hz oscillations synchronize prefrontal-amygdala circuits during fear behavior [Internet]. Nat Neurosci 2016; 19; 605–12. Available from: http://www.nature.com.proxy.lib.uiowa.edu/neuro/journal/vaop/ncurrent/full/nn.4251.html [25 February 2016, date last accessed].

Kim Y-C, Han S-W, Alberico SL, Ruggiero RN, De Corte B, Chen K-H, et al. Optogenetic stimulation of frontal D1 neurons compensates for impaired temporal control of action in dopamine-depleted mice. Curr Biol 2017; 27: 39–47.

Kingyon J, Behroozmand R, Kelley R, Oya H, Kawasaki H, Narayanan NS, et al. High-gamma band fronto-temporal coherence as a measure of functional connectivity in speech motor control. Neuroscience 2015; 305: 15–25.

Laubach M, Caetano MS, Narayanan NS. Mistakes were made: neural mechanisms for the adaptive control of action initiation by the medial prefrontal cortex [Internet]. J Physiol 2015; 109: 104–17. Available from: http://www.sciencedirect.com/science/article/pii/S0928425715000029 [5 February 2015, date last accessed].

Limousin P, Krack P, Pollak P, Benazzouz A, Ardouin C, Hoffmann D, et al. Electrical stimulation of the subthalamic nucleus in advanced Parkinson's disease. N Engl J Med 1998; 339: 1105–11.

Logothetis N. Intracortical recordings and fMRI: an attempt to study operational modules and networks simulatneously. Neuroimage 2012; 62: 962–9.

Logothetis N, Augath M, Murayama Y, Rauch A, Sultan F, Goense J, et al. The effects of electrical microstimulation on cortical signal propagation. Nat Neurosci 2010; 13: 1283–91.

Malapani C, Rakitin BC. Interval timing in the dopamine-depleted basal ganglia: from empirical data to timing theory. In: Functional and neural mechanisms of interval timing. Boca Raton, FL: CRC Press; 2003. p. 485–514.

Mathai A, Smith Y. The corticostriatal and corticosubthalamic pathways: two entries, one target. So what? Front Syst Neurosci 2011; 5: 64.

Nambu A, Tokuno H, Takada M. Functional significance of the cortico-subthalamo-pallidal 'hyperdirect' pathway. Neurosci Res 2002; 43: 111–17.

Narayanan NS, Cavanagh JF, Frank MJ, Laubach M. Common medial frontal mechanisms of adaptive control in humans and rodents. Nat Neurosci 2013a; 16: 1888–97.

Narayanan NS, Land BB, Solder JE, Deisseroth K, DiLeone RJ. Prefrontal D1 dopamine signaling is required for temporal control. Proc Natl Acad Sci USA 2012; 109: 20726–31.

Narayanan NS, Rodnitzky RL, Uc EY. Prefrontal dopamine and cognitive symptoms of Parkinson's disease. Rev Neurosci 2013b; 24: 267–78.

Okun MS, Fernandez HH, Wu SS, Kirsch-Darrow L, Bowers D, Bova F, et al. Cognition and mood in Parkinson's disease in subthalamic nucleus versus globus pallidus interna deep brain stimulation: the COMPARE trial. Ann Neurol 2009; 65: 586–95.

Oya H, Howard MA, Magnotta VA, Kruger A, Griffiths TD, Lemieux L, et al. Mapping effective connectivity in the human brain with concurrent intracranial electrical stimulation and BOLD-fMRI. J Neurosci Methods 2017; 277: 101–12.

Parker KL, Kim Y, Kelley RM, Nessler AJ, Chen K-H, Muller-Ewald VA, et al. Delta-frequency stimulation of cerebellar projections can compensate for schizophrenia-related medial frontal dysfunction. Molecular Psychiatry 2017: 647–55.

Parker KL, Chen K-H, Kingyon JR, Cavanagh JF, Narayanan NS. D1-Dependent 4 Hz oscillations and ramping activity in rodent medial frontal cortex during interval timing. J Neurosci 2014; 34: 16774–83.

Parker KL, Chen K-H, Kingyon JR, Cavanagh JF, Naryanan NS. Medial frontal ~4 Hz activity in humans and rodents is attenuated in PD patients and in rodents with cortical dopamine depletion. J Neurophysiol 2015; 114: 1310–20.

Parker KL, Lamichhane D, Caetano MS, Narayanan NS. Executive dysfunction in Parkinson's disease and timing deficits. Front Integr Neurosci 2013; 7: 75.

Ridderinkhof KR, Ullsperger M, Crone EA, Nieuwenhuis S. The role of the medial frontal cortex in cognitive control. Science 2004; 306: 443–7.

Rosenberg JR, Amjad AM, Breeze P, Brillinger DR, Halliday DM. The Fourier approach to the identification of functional coupling between neuronal spike trains. Prog Biophys Mol Biol 1989; 53: 1–31.

Swadlow HA, Waxman SG. Variations in conduction velocity and excitability following single and multiple impulses of visual callosal axons in the rabbit. Exp Neurol 1976; 53: 128–50.

Voon V, Fox SH. Medication-related impulse control and repetitive behaviors in Parkinson disease. Arch Neurol 2007; 64: 1089–96.

Wessel JR, Aron AR. On the Globality of Motor Suppression: unexpected events and their influence on behavior and cognition. Neuron 2017; 93: 259–80.

Wessel JR, Jenkinson N, Brittain J-S, Voets SHEM, Aziz TZ, Aron AR. Surprise disrupts cognition via a fronto-basal ganglia suppressive mechanism. Nat Commun 2016; 7: 11195.

Wojtecki L, Elben S, Timmermann L, Reck C, Maarouf M, Jorgens S, et al. Modulation of human time processing by subthalamic deep brain stimulation [Internet]. PLoS One 2011; 6: e24589. Available from: http://www.ncbi.nlm.nih.gov/pmc/articles/PMC3171456/ [5 June 2014, date last accessed].

Zaghloul KA, Weidemann CT, Lega BC, Jaggi JL, Baltuch GH, Kahana MJ. Neuronal activity in the human subthalamic nucleus encodes decision conflict during action selection. J Neurosci 2012; 32: 2453–60.

Zavala BA, Tan H, Little S, Ashkan K, Hariz M, Foltynie T, et al. Midline frontal cortex low-frequency activity drives subthalamic nucleus oscillations during conflict. J Neurosci 2014; 34: 7322–33.

Zavala B, Brittain J-S, Jenkinson N, Ashkan K, Foltynie T, Limousin P, et al. Subthalamic nucleus local field potential activity during the Eriksen flanker task reveals a novel role for theta phase during conflict monitoring. J Neurosci 2013; 33: 14758–66.

Zavala B, Tan H, Ashkan K, Foltynie T, Limousin P, Zrinzo L, et al. Human subthalamic nucleus-medial frontal cortex theta phase coherence is involved in conflict and error related cortical monitoring. Neuroimage 2016; 137: 178–87.